JACS
JOURNAL OF THE AMERICAN CHEMICAL SOCIETY
pubs.acs.org/JACS
Communication

Tailoring the Interfacial Interactions of van der Waals 1T-MoS_2/C_{60} Heterostructures for High-Performance Hydrogen Evolution Reaction Electrocatalysis

Alain R. Puente Santiago,*,⊗ Tianwei He,⊗ Oscar Eraso, Md Ariful Ahsan, Aruna N. Nair, Venkata S. N. Chava, Ting Zheng, Srikanth Pilla, Olivia Fernandez-Delgado, Aijun Du, Sreeprasad T. Sreenivasan,* and Luis Echegoyen*

Cite This: J. Am. Chem. Soc. 2020, 142, 17923−17927
Read Online
ACCESS | Metrics & More | Article Recommendations | Supporting Information

ABSTRACT: Fullerene-based low-dimensional (LD) heterostructures have emerged as excellent energy conversion materials. We constructed van der Waals 1T-MoS_2/C_{60} 0D-2D heterostructures via a one-pot synthetic approach for catalytic hydrogen generation. The interfacial 1T-MoS_2−C_{60} and C_{60}−C_{60} interactions as well as their electrocatalytic properties were finely controlled by varying the weight percentages of the fullerenes. 1T-MoS_2 platforms provided a novel template for the formation of C_{60} nanosheets (NSs) within a very narrow fullerene concentration range. The heterostructure domains of 1T-MoS_2 and C_{60} NSs exhibited excellent hydrogen evolution reaction (HER) performances, with one of the lowest onset potentials and ΔG_{H^*} values for LD non-precious nanomaterials reported to date.

In the past decade, hydrogen has become a significant competitor as a stable and non-carbon energy source in the renewable energy grid.[1,2] The conventional methods of hydrogen production are still very far from reaching the standards for energy sustainability. Thus, the development of green and clean technologies to boost the hydrogen economy is of paramount importance. In this direction, water splitting processes represent a sustainable approach to obtaining hydrogen, which has triggered the development of advanced electrolyzer technologies using different types of catalytic materials.[3] Noble metals catalyze the electrochemical generation of hydrogen at ultralow overpotential values,[4] but their high prices and scarcity are important drawbacks. Therefore, the discovery of Earth-abundant hydrogen evolution reaction (HER) catalysts with very low overpotentials is highly desirable.[5,6]

Molybdenum disulfide (MoS_2) has been widely investigated as a promising electrocatalyst for HER.[7,8] It has been theoretically and experimentally confirmed that the sulfur edge domains of 2H-MoS_2 nanosheets (NSs) exhibit high catalytic activities towards hydrogen electrocatalysis, while the basal planes remain largely inactive.[9,10] Efforts to maximize the number of catalytically active sites vary from the addition of thiomolybdate nanoclusters, an artificial sub-monolayer of edge sulfur atoms, to the MoS_2 network[11] and the creation of S-vacancies in the basal planes,[12] to the conversion of the semiconductor 2H phase into metallic 1T phase MoS_2 NSs.[13,14] Despite all these breakthroughs, the activation and optimization of the HER electrocatalytic activity on MoS_2 nanostructures via their hybridization with low-dimensional (LD) materials has been scarcely investigated.[15] Buckminsterfullerenes constitute promising candidates to form electrocatalytic MoS_2/C_{60} heterostructures due to their ability to induce intermolecular charge transfer processes, thus creating highly active interfacial catalytic active sites.[16]

In this work, we have drastically improved the electrocatalytic HER properties of van der Waals (vdW) 1T-MoS_2/C_{60} heterostructures by the formation of well-organized arrays of C_{60} molecules in a very narrow fullerene concentration range. The catalytic performances of the 1T-MoS_2/C_{60} were nicely tailored by varying the fullerene weight percentages. We have also prepared 2H-MoS_2/C_{60} materials to compare the effect of the MoS_2 phase on the electrocatalytic performance. The modulation of the MoS_2−C_{60} and C_{60}−C_{60} interactions at specific ratios seems to be the driving force to form highly active HER catalysts that yielded an optimal ΔG_H = −0.03 eV value, which allowed us to achieve one of the lowest onset overpotential values among LD non-precious HER nanomaterials. This is the first time, to the best of our knowledge, that the structure/catalytic function relationship of fullerene-based LD nanomaterials is reported using a framework of experimental and theoretical techniques.

vdW MoS_2/C_{60} heterostructures were synthesized using a one-pot strategy (Figure 1a) to accomplish the non-covalent functionalization with different C_{60} weight contents (from 5% to 95%) onto 1T- and 2H-MoS_2 NSs (see the Supporting Information for synthetic details and Figure S1). The resulting 1T-MoS_2/C_{60} heterostructures were characterized by a multi-

Received: August 17, 2020
Published: October 8, 2020

https://dx.doi.org/10.1021/jacs.0c08867
J. Am. Chem. Soc. 2020, 142, 17923−17927

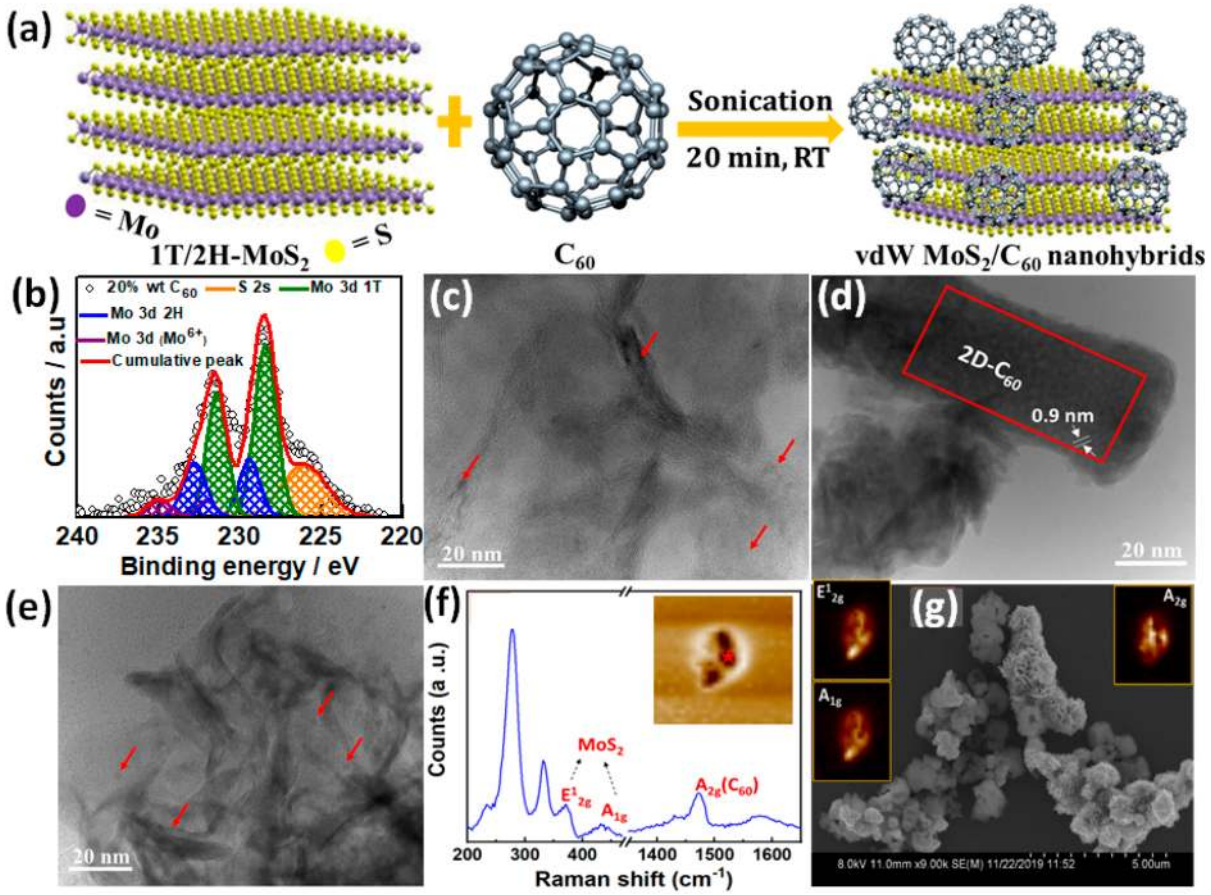

Figure 1. (a) Schematic representation of the synthesis of the MoS_2/C_{60} heterostructure. (b) Mo 3d and S 2s XPS bands of the 1T-MoS_2/20 wt% C_{60} heterostructure. HRTEM images of (c) 1T-MoS_2/5 wt% C_{60}, (d) 1T-MoS_2/20 wt% C_{60}, and (e) 1T-MoS_2/80 wt% C_{60}. (f) Representative Raman spectrum of a MoS_2 and C_{60} heterostructure sample. The inset shows the 2D spectrum of the sample region from which the Raman spectrum image is recorded. (g) SEM image of the same sample region shown in the inset of (f). The insets show the 2D maps of the corresponding E^1_{2g}, A_{1g}, and A_{2g} modes of the MoS_2 and C_{60} regions.

techique approach. Raman spectroscopy revealed that the typical pinch-mode band of C_{60} at ca. 1480 cm^{-1} as well as the two characteristic in-plane (E^1_{2g}) and out-of-plane (A_{1g}) Raman bands of MoS_2 nanosheets were shifted in the heterostructures (Figure S2), suggesting pronounced interfacial interactions between C_{60} and MoS_2 layers.[17] High-resolution spectra from the X-ray photoelectron spectroscopy (XPS) analysis of the Mo 3d region revealed that 1T is the main phase of the MoS_2 in the heterostructures (Figure 1b, Figure S3). The Mo 3d spectra showed features corresponding to the $3d_{5/2}$ and $3_{3/2}$ contributions of 1T-MoS_2, located at 228 and 231.2 eV, respectively.[18] High-resolution transmission electron microscopy (HRTEM) displayed unique morphological features for the materials formed from 20 wt% of C_{60}. Fullerenes adopted cluster-like or well-dispersed distributions in mostly all the MoS_2/C_{60} ratios explored (Figure 1c,e), while they formed well-ordered 2D arrays at a specific C_{60} weight content around 20% (Figure 1d). These findings suggest that the 1T-MoS_2 nanosheets act as templates for the nucleation and subsequent growth of fullerene 2D NSs at 20 wt% of fullerenes. The unique growth of C_{60} NSs on 1T-MoS_2 surfaces is linked to the modulation, at specific ratios, of the MoS_2-C_{60} and $C_{60}-C_{60}$ interfacial interactions, which minimize the aggregation of fullerenes, thus optimizing their two-dimensional growth to a self-assembly process on the top of the 1T-MoS_2 surfaces.[19] Scanning electron microscopy (SEM) and energy-dispersive spectroscopy (EDS) measurements have confirmed the presence of two different domains in the 20 wt% C_{60} heterostructures (Figure S4). They are composed of C_{60} NSs and 2D-2D 1T-MoS_2/C_{60} NSs. The last ones most likely form MoS_2/C_{60} NS/MoS_2 sandwich-like frameworks. This was further verified using Raman mapping experiments, which were employed to probe the vibrational modes of the different domains in the 1T-MoS_2/C_{60} structures. A two-dimensional (2D) Raman spectrum map was recorded from a sample region that was imaged using SEM by excitation at 532 nm (Figure 1f,g). Figure 1f shows a representative Raman spectrum corresponding to the region marked in the 2D spectrum (inset). The peaks at 380 and 405 cm^{-1} correspond to E^1_{2g} and A_{1g} vibrational modes of MoS_2, whereas the peak at 1460 cm^{-1} corresponds to the A_{2g} mode or pentagonal pinch mode of C_{60}. Further, we reconstructed 2D Raman maps of E^1_{2g}, A_{1g} of MoS_2 and A_{2g} of C_{60} (see Figure 1g). These images show that the A_{2g} peak intensity of C_{60} is higher in the area where we observed C_{60} nanosheet-like features using SEM, and the E^1_{2g} and A_{1g} modes of MoS_2 show higher intensities in the other parts of the heterostructure region, which correspond to the 2D-2D 1T-MoS_2/C_{60} NS domains.

To investigate the effects of the C_{60} adsorption patterns on the HER electrocatalytic behavior of our 1T-MoS_2/C_{60} nanomaterials, we carried out linear sweep voltammetry (LSV) measurements in 0.5 M H_2SO_4. As a benchmark, we

https://dx.doi.org/10.1021/jacs.0c08867
J. Am. Chem. Soc. 2020, 142, 17923−17927

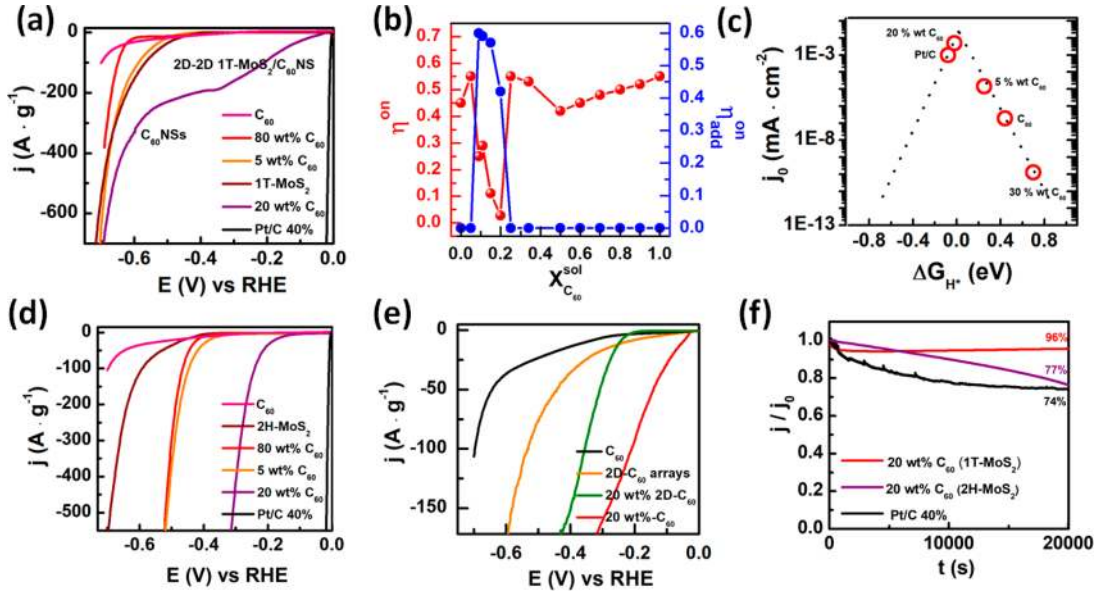

Figure 2. (a) Mass-normalized catalytic currents for C_{60}, 1T-MoS_2, commercial Pt/C 40%, and the 1T-MoS_2/C_{60} heterostructures with 5, 20, and 80 wt% of C_{60} at 2 mV·s^{-1} in 0.5 M H_2SO_4. (b) HER onset overpotential values as a function of the C_{60} volume fraction in solution. (c) Volcano plots of the as-synthesized vdW 1T-MoS_2/C_{60}. (d) Mass-normalized catalytic currents for C_{60}, 2H-MoS_2, commercial Pt/C 40%, and the 2H-MoS_2/C_{60} heterostructures with 5, 20, and 80 wt% of C_{60} at 2 mV·s^{-1} in 0.5 M H_2SO_4. (e) Mass-normalized LSVs for C_{60}, C_{60} NSs, 20 wt% 2D-C_{60}, and 20 wt% C_{60} at 2 mV·s^{-1} in 0.5 M H_2SO_4. (f) Chronoamperometric curves of 2H-MoS_2/20 wt% C_{60} and 1T-MoS_2/20 wt% C_{60} at −0.35 V vs RHE.

have also characterized the catalytic performance of commercial Pt/C, which exhibited a near-zero HER overpotential. Figure 2a,d shows the LSVs of both 1T-MoS_2/C_{60} and 2H-MoS_2/C_{60} heterostructures constructed using 5, 20, and 80 wt% of C_{60}, where the catalytic currents were normalized by the mass of the nano-heterostructures to obtain a deeper understanding of their intrinsic catalytic activities. The polarization curves recorded with the 1T-MoS_2/C_{60} nanocatalytic system displayed unique electrochemical features (Figure 2a). The onset potentials of the structures were plotted as a function of the C_{60} weight content (Figure 2b). As shown, the appearance of an additional onset potential value took place in a low range of fullerene concentrations, mostly between 8% and 20% (Figure S5). Particularly, the 20 wt% C_{60} vdW heterostructures exhibit two well-defined catalytic waves, which, to the best of our knowledge, have not been reported for HER processes. This unusual catalytic behavior has been detected for other water-splitting reactions.[20] For instance, the oxygen electroreduction of laccase−AuNPs nanosystems displayed two electrocatalytic contributions, which were ascribed to the different electronic wiring properties of laccases adsorbed onto nanoparticles and glassy carbon (GC) surfaces.[20] It is worth noting that the first electrocatalytic process shows an ultrasmall onset potential of −0.027 V vs RHE, which is better than the catalytic activity of their individual components and is comparable with those using Pt/C (−0.004 V vs RHE) and other state-of-the-art HER catalysts (Table S1), while the second catalytic onset potential is −0.42 V vs RHE, which is also better than those of the other heterostructures. Accordingly, the 1T-MoS_2/20 wt% C_{60} displayed two Tafel slopes (Figure S6). The smaller slope, which belongs to the first catalytic wave (57 mV·s^{-1}), is by far the value closer to that obtained with Pt/C (35 mV·s^{-1}) among all the heterostructures, demonstrating their electrokinetic efficiency. Electrochemical impedance spectroscopy (EIS) plots further confirmed the faster electron transfer kinetics of the 1T-MoS_2/20 wt% C_{60} heterostructures (Figure S7), which exhibited a lower charge resistance value (19 Ω). Additionally, the volcano plots revealed that 1T-MoS_2/20 wt% C_{60} has almost the same position as Pt/C, close to the peak, indicating a Pt-like catalytic activity (Figure 2c). We have observed similar catalytic trends using 2H-MoS_2 platforms to form the heterostructures (Figure 2d). 2H-MoS_2/20%wt C_{60} was the heterostructure with the most effective onset overpotential value (−0.17 vs RHE). As it was revealed in the microscopic characterization, the 20 wt% C_{60} nanoheterostructures show the presence of well-ordered fullerene nanosheets that are either forming free-MoS_2 domains or intercalated into the MoS_2 layers. To get in-depth electrocatalytic information on these interesting LD materials, the LSVs of C_{60} NSs and C_{60} NSs physically mixed with 1T-MoS_2 layers (20 wt% 2D-C_{60}) were obtained (Figure 2e, Figure S8). The onset overpotentials of both nanostructures are larger than the onset overpotential of the first 20 wt% C_{60} catalytic wave, suggesting that the 2D-2D 1T-MoS_2/C_{60} NS domains are responsible for the most efficient HER electrocatalysis. Also, the onset potentials of the as-synthesized C_{60} NSs (−0.36 V vs RHE) and the second electrocatalytic wave are very similar, which indicates that the lower catalytic efficiency occurs at the C_{60} NS domains. These findings can be understood on the basis of (i) the interconnected conductive 2D-2D 1T-MoS_2/C_{60} NS network, which promotes faster electron transfer rates from the glassy carbon electrodes to the catalytically active sites, confirmed by the lower R_{CT}, and (ii) its optimal interfacial interactions that decrease the uphill energy states of each catalytic step, thus improving the HER performance. The 1T-MoS_2/20 wt% C_{60} structures delivered excellent stability, keeping 96% of the initial current density after 20 000 s, thus surpassing the stability of Pt/C (Figure 2f).

https://dx.doi.org/10.1021/jacs.0c08867
J. Am. Chem. Soc. 2020, 142, 17923−17927

To further understand the catalytic performance of the 1T-MoS_2/C_{60} nanostructures and unravel the origin of the excellent catalytic activity of the 2D-2D 1T-MoS_2/C_{60} NS domains, density functional theory (DFT) calculations (see Supporting Information for computational details) were performed. Different C_{60} weight percentages (5%, 20%, and 30%) were added onto 1T-MoS_2 surfaces (Figure 3a, Figure S9) to simulate the 1T-MoS_2/C_{60} interfaces. First, the HER active sites of the 1T-MoS_2/C_{60} nanostructures were identified by calculating the binding energies of the adsorbed hydrogen at different sites. The binding strength of the hydrogen on top of the C_{60} (0.74 eV) and on the in-plane MoS_2 (1.81 eV) were very weak, which leads to low kinetics for H* generation. On the other hand, the C atoms located at the 1T-MoS_2/C_{60} interfaces exhibited moderate binding energy values (−0.33 eV), indicating that they are the active catalytic sites for the HER process, as is stated by the Sabatier principle.[21] Second, the charge density differences of the 1T-MoS_2/C_{60} nanostructures were calculated (Figure 3b). The results suggest that the charge transfer process mainly takes place from the C atoms at the interface of the composite to the in-plane MoS_2, which is in good agreement with previous reports.[17,22] Such charge transfer could also polarize the Mo−S bonds, which decreases the enthalpy for hydrogen adsorption, thus giving rise to active HER sites at the 1T-MoS_2/C_{60} interfaces.[22] Importantly, the density of states of the 2D-2D 1T-MoS_2/C_{60} NS domain was analyzed (Figure 3c). It showed that the electronic states of C atoms are overlapped with those of the Mo and S atoms, implying effective interfacial interactions between the C_{60} and MoS_2. Based on these facts, we believe that the 1T-MoS_2/C_{60} interfacial interactions are mainly based on both vdW and weak covalent interactions. The large number of electronic states close to the Fermi level indicates high electroconductivity and carrier density at the 1T-MoS_2/C_{60} NS interfaces, which strongly supports our experimental results. Figure 3d displays the ΔG_{H^*} values for the heterostructures with 5%, 20%, and 30% of C_{60} as well as the pristine C_{60} and the MoS_2 edges. As is well known, the ideal HER catalyst requires a value of ΔG_{H^*} close to zero.[23,24] It is clear that the 2D-2D 1T-MoS_2/C_{60} NS structure (ΔG_{H^*} = −0.03 eV) exhibits the best HER catalytic activity, outperforming both pristine C_{60} (ΔG_{H^*} = 0.44 eV) and MoS_2 edges (ΔG_{H^*} = 0.08 eV) as well as the other two heterostructures, placing it among the five best-performing HER catalysts (Table S2). This is attributed to the moderate interfacial interactions between the C_{60} and MoS_2, which lead to optimal binding strengths of H atoms on the active sites.

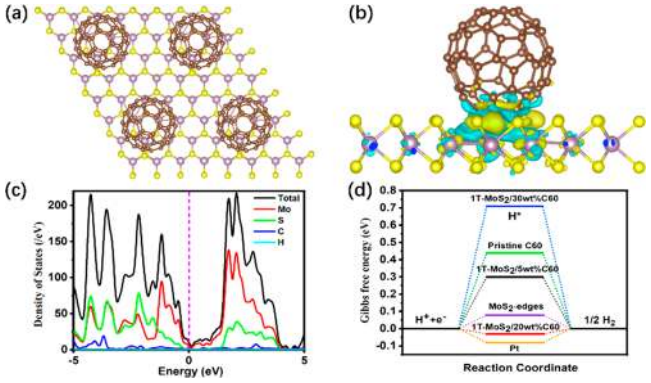

Figure 3. (a) Top view of the optimized model and (b) the calculated charge density difference for the 1T-MoS_2/C_{60} heterostructures. (c) Total electronic density of states for 2D-2D domains of the MoS_2/20 wt% C_{60} heterostructure (pink dashed line represents the Fermi level). (d) Calculated HER free energy diagrams. Color code in (a) and (b): S, yellow; Mo, light violet; C, brown.

In summary, we have demonstrated that the structural and catalytic properties of 1T-MoS_2/C_{60} heterostructures can be tuned at the nanoscale level by changing the C_{60} weight contents via a simple synthetic strategy. 1T-MoS_2/C_{60} materials with 20 wt% C_{60} showed different fullerene arrangements, which were directly connected to the two catalytic HER waves. The 2D-2D 1T-MoS_2/C_{60} NSs domains exhibited impressive catalytic performances, rendering Pt-like onset potentials and ultralow ΔG_{H^*} values. This work provides in-depth insights into the rational design of highly active non-precious 0D-2D catalysts.

■ ASSOCIATED CONTENT

Supporting Information

The Supporting Information is available free of charge at https://pubs.acs.org/doi/10.1021/jacs.0c08867.

Synthetic strategy details; structural characterization of the MoS_2nanoplatforms; Raman and XPS spectra of the heterostructures; LSVs of 1T-MoS_2/C_{60} with different fullerene weight contents; Tafel plots; Nyquist plots for the 1T-MoS_2/C_{60} heterostructures; SEM of C_{60} NSs; computational details (PDF)

■ AUTHOR INFORMATION

Corresponding Authors

Alain R. Puente Santiago − *Department of Chemistry, University of Texas at El Paso, El Paso, Texas 79968, United States;* orcid.org/0000-0002-8491-3565; Email: arpuentesan@utep.edu

Sreeprasad T. Sreenivasan − *Department of Chemistry, University of Texas at El Paso, El Paso, Texas 79968, United States;* orcid.org/0000-0002-5728-0512; Email: sreenivasan@utep.edu

Luis Echegoyen − *Department of Chemistry, University of Texas at El Paso, El Paso, Texas 79968, United States;* orcid.org/0000-0003-1107-9423; Email: echegoyen@utep.edu

Authors

Tianwei He − *School of Chemistry and Physics, Science and Engineering Faculty and Centre for Materials Science, Queensland University of Technology, Brisbane, QLD 4000, Australia*

Oscar Eraso − *Department of Chemistry, University of Texas at El Paso, El Paso, Texas 79968, United States*

Md Ariful Ahsan − *Department of Chemistry, University of Texas at El Paso, El Paso, Texas 79968, United States;* orcid.org/0000-0002-2024-8690

Aruna N. Nair − *Department of Chemistry, University of Texas at El Paso, El Paso, Texas 79968, United States*

Venkata S. N. Chava − *Department of Chemistry, University of Texas at El Paso, El Paso, Texas 79968, United States*

Ting Zheng − *Department of Automotive Engineering, Clemson Composites Center, and Department of Materials Science and Engineering, Clemson University, Greenville, South Carolina 29607, United States;* orcid.org/0000-0002-4115-4626

https://dx.doi.org/10.1021/jacs.0c08867
J. Am. Chem. Soc. 2020, 142, 17923−17927

Srikanth Pilla − *Department of Automotive Engineering, Clemson Composites Center, Department of Materials Science and Engineering, and Department of Mechanical Engineering, Clemson University, Greenville, South Carolina 29607, United States;* orcid.org/0000-0003-3728-6578

Olivia Fernandez-Delgado − *Department of Chemistry, University of Texas at El Paso, El Paso, Texas 79968, United States;* orcid.org/0000-0002-6641-026X

Aijun Du − *School of Chemistry and Physics, Science and Engineering Faculty and Centre for Materials Science, Queensland University of Technology, Brisbane, QLD 4000, Australia;* orcid.org/0000-0002-3369-3283

Complete contact information is available at: https://pubs.acs.org/10.1021/jacs.0c08867

Author Contributions

⊗A.R.P.S. and T.H. contributed equally to this work.

Notes

The authors declare no competing financial interest.

■ ACKNOWLEDGMENTS

L.E. would like to thank the NSF for the generous support of this work under CHE-1801317. The Robert A. Welch Foundation is also gratefully acknowledged for an endowed chair to L.E. (grant AH-0033). S.T.S. acknowledges the financial support from UTEP start-up grant, UT STARs award, UTEP-URI award, and the U.S. National Science Foundation (NSF) PREM grant #DMR-1827745.

■ REFERENCES

(1) Glenk, G.; Reichelstein, S. Economics of converting renewable power to hydrogen. *Nat. Energy* **2019**, *4* (3), 216−222.
(2) Tanc, B.; Arat, H. T.; Baltacioglu, E.; Aydin, K. Overview of the next quarter century vision of hydrogen fuel cell electric vehicles. *Int. J. Hydrogen Energy* **2019**, *44* (20), 10120−10128.
(3) El-Emam, R. S.; Ozcan, H. Comprehensive review on the techno-economics of sustainable large-scale clean hydrogen production. *J. Cleaner Prod.* **2019**, *220*, 593−609.
(4) Ren, X. F.; Lv, Q. Y.; Liu, L. F.; Liu, B. H.; Wang, Y. R.; Liu, A. M.; Wu, G. Current progress of Pt and Pt-based electrocatalysts used for fuel cells. *Sustain. Energy Fuels* **2020**, *4* (1), 15−30.
(5) Roger, I.; Shipman, M. A.; Symes, M. D. Earth-abundant catalysts for electrochemical and photoelectrochemical water splitting. *Nat. Rev. Chem.* **2017**, *1* (1), 0003.
(6) Kibsgaard, J.; Chorkendorff, I. *Nat. Energy* **2019**, *4* (6), 430−433.
(7) Jiao, Y. C.; Hafez, A. M.; Cao, D. X.; Mukhopadhyay, A.; Ma, Y.; Zhu, H. L. Metallic MoS_2 for high performance energy storage and energy conversion. *Small* **2018**, *14* (36), 1800640.
(8) Jayabal, S.; Saranya, G.; Wu, J.; Liu, Y. Q.; Geng, D. S.; Meng, X. B. Understanding the high-electrocatalytic performance of two-dimensional MoS_2 nanosheets and their composite materials. *J. Mater. Chem. A* **2017**, *5* (47), 24540−24563.
(9) Jaramillo, T. F.; Jorgensen, K. P.; Bonde, J.; Nielsen, J. H.; Horch, S.; Chorkendorff, I. Identification of active edge sites for electrochemical H_2 evolution from MoS_2 nanocatalysts. *Science* **2007**, *317* (5834), 100−102.
(10) Hinnemann, B.; Moses, P. G.; Bonde, J.; Jorgensen, K. P.; Nielsen, J. H.; Horch, S.; Chorkendorff, I.; Norskov, J. K. Biomimetic hydrogen evolution: MoS_2 nanoparticles as catalyst for hydrogen evolution. *J. Am. Chem. Soc.* **2005**, *127* (15), 5308−5309.
(11) Kibsgaard, J.; Jaramillo, T. F.; Besenbacher, F. Building an appropriate active-site motif into a hydrogen-evolution catalyst with thiomolybdate $[Mo_3S_{13}]^{2-}$ clusters. *Nat. Chem.* **2014**, *6* (3), 248−253.
(12) Li, H.; Tsai, C.; Koh, A. L.; Cai, L. L.; Contryman, A. W.; Fragapane, A. H.; Zhao, J. H.; Han, H. S.; Manoharan, H. C.; Abild-Pedersen, F.; Norskov, J. K.; Zheng, X. L. Activating and optimizing MoS_2 basal planes for hydrogen evolution through the formation of strained sulphur vacancies. *Nat. Mater.* **2016**, *15* (1), 48−53.
(13) Lukowski, M. A.; Daniel, A. S.; Meng, F.; Forticaux, A.; Li, L. S.; Jin, S. Enhanced hydrogen evolution catalysis from chemically exfoliated metallic MoS_2 nanosheets. *J. Am. Chem. Soc.* **2013**, *135* (28), 10274−10277.
(14) Liu, Q.; Li, X. L.; He, Q.; Khalil, A.; Liu, D. B.; Xiang, T.; Wu, X. J.; Song, L. Gram-scale aqueous synthesis of stable few-layered 1T-MoS_2: applications for visible-light-driven photocatalytic hydrogen evolution. *Small* **2015**, *11* (41), 5556−5564.
(15) Liu, Q.; Fang, Q.; Chu, W. S.; Wan, Y. Y.; Li, X. L.; Xu, W. Y.; Habib, M.; Tao, S.; Zhou, Y.; Liu, D. B.; Xiang, T.; Khalil, A.; Wu, X. J.; Chhowalla, M.; Ajayan, P. M.; Song, L. Electron-doped 1T-MoS_2 via interface engineering for enhanced electrocatalytic hydrogen evolution. *Chem. Mater.* **2017**, *29* (11), 4738−4744.
(16) Gao, R.; Dai, Q. B.; Du, F.; Yan, D. P.; Dai, L. M. C_{60}-adsorbed single-walled carbon nanotubes as metal-free, ph-universal, and multifunctional catalysts for oxygen reduction, oxygen evolution, and hydrogen evolution. *J. Am. Chem. Soc.* **2019**, *141* (29), 11658−11666.
(17) Chen, R. F.; Lin, C.; Yu, H.; Tang, Y. T.; Song, C.; Yuwen, L. H.; Li, H.; Xie, X. J.; Wang, L. H.; Huang, W. Templating C_{60} on MoS_2 nanosheets for 2D hybrid Van der Waals p−n nano-heterojunctions. *Chem. Mater.* **2016**, *28* (12), 4300−4306.
(18) Geng, X. M.; Sun, W. W.; Wu, W.; Chen, B.; Al-Hilo, A.; Benamara, M.; Zhu, H. L.; Watanabe, F.; Cui, J. B.; Chen, T. P. Pure and stable metallic phase molybdenum disulfide nanosheets for hydrogen evolution reaction. *Nat. Commun.* **2016**, *7*, 10672.
(19) Tian, H.; Zhu, S. Y.; Xu, F. G.; Mao, W. T.; Wei, H.; Mai, Y. Y.; Feng, X. L. Growth of 2D mesoporous polyaniline with controlled pore structures on ultrathin MoS_2 nanosheets by block copolymer self-assembly in solution. *ACS Appl. Mater. Interfaces* **2017**, *9* (50), 43975−43982.
(20) Gutierrez-Sanchez, C.; Pita, M.; Vaz-Dominguez, C.; Shleev, S.; De Lacey, A. L. Gold nanoparticles as electronic bridges for laccase-based biocathodes. *J. Am. Chem. Soc.* **2012**, *134* (41), 17212−17220.
(21) Medford, A. J.; Vojvodic, A.; Hummelshoj, J. S.; Voss, J.; Abild-Pedersen, F.; Studt, F.; Bligaard, T.; Nilsson, A.; Norskov, J. K. From the Sabatier principle to a predictive theory of transition-metal heterogeneous catalysis. *J. Catal.* **2015**, *328*, 36−42.
(22) Choi, Y. H.; Lee, J.; Parija, A.; Cho, J. S.; Verkhoturov, S. V.; Al-Hashimi, M.; Fang, L.; Banerjee, S. An in situ sulfidation approach for the integration of MoS_2 nanosheets on carbon fiber paper and the modulation of its electrocatalytic activity by interfacing with nC_{60}. *ACS Catal.* **2016**, *6* (9), 6246−6254.
(23) He, T. W.; Gao, G. P.; Kou, L. Z.; Will, G.; Du, A. J. Endohedral metallofullerenes ($M@C_{60}$) as efficient catalysts for highly active hydrogen evolution reaction. *J. Catal.* **2017**, *354*, 231−235.
(24) Craig, M. J.; Coulter, G.; Dolan, E.; Soriano-Lopez, J.; Mates-Torres, E.; Schmitt, W.; Garcia-Melchor, M. Garcia-Melchor. Universal scaling relations for the rational design of molecular water oxidation catalysts with near-zero overpotential. M. *Nat. Commun.* **2019**, *10*, 4993.